Surface & Coatings Technology 304 (2016) 438–449

Contents lists available at ScienceDirect

Surface & Coatings Technology

journal homepage: www.elsevier.com/locate/surfcoat

Characterization of PEO nanocomposite coatings on titanium formed in electrolyte containing atenolol

Hossein Sharifi, M. Aliofkhazraei *, Ghasem Barati Darband, A. Sabour Rouhaghdam

Department of Materials Engineering, Faculty of Engineering, Tarbiat Modares University, P.O. Box: 14115-143, Tehran, Iran

ARTICLE INFO

Article history:
Received 6 April 2016
Revised 30 June 2016
Accepted in revised form 16 July 2016
Available online 18 July 2016

Keywords:
PEO nanocomposite
Atenolol
Corrosion
EIS
Wear
Nanoindentation

ABSTRACT

Nanocomposite coatings were formed on commercial pure titanium through plasma electrolytic oxidation (PEO) process in a phosphate-based electrolyte containing atenolol and alumina nanoparticles. The procedure was performed by direct current and current density was kept constant. The effects of atenolol concentration in the electrolyte on growth of coatings, absorption of alumina nanoparticles, morphology, chemical and physical structure and corrosion and mechanical behavior of coatings were studied by dynamic light scattering spectroscopy, scanning electron microscopy, energy dispersion X-ray spectroscopy, X-ray diffraction, potentiodynamic polarization test, electrochemical impedance spectroscopy, nanoindentation and pin-on-disk wear test. The existence of atenolol in the electrolyte was observed to increase the diffusion depth of alumina nanoparticles and decrease porosity. This behavior, in turn, led to an increase in charge transfer resistance by 211,420 Ω cm^2. Moreover, the addition of atenolol in alumina suspension decreased the wear rate by 130 times as it increased absorption of alumina nanoparticles and improved mechanical properties.

1. Introduction

Titanium and titanium-based alloys are widely applied in aerospace, petrochemical, and biomedical industries because of their distinguished properties such as high strength to weight ratio, high melting temperature, appropriate mechanical properties, high resistance to corrosion, and biocompatibility [1]. To further improve titanium function in terms of mechanical properties, corrosion resistance, and biocompatibility, the rather new method of plasma electrolytic oxidation has recently been paid a great deal of attention [2]. The parameters of coating process which may be varied to achieve the best desired properties mainly consist of the electrolyte effect and electrical parameters of the PEO process. Among these parameters, the electrolyte and its additives are of great importance in the PEO process because of the role of their components in sparking process as well as the introduction of elements into the coating and affecting its properties. Recent studies regarding electrolyte and PEO process are mostly dedicated to the electrolyte additive effects [3,4]. It was reported that addition of cerium nitrate to the PEO electrolyte on titanium leads to the formation of a coating with proper biocompatibility properties [5]. The existence of sodium vanadate in the PEO electrolyte on titanium was seen to improve photocatalytic properties [6]. Moreover, the existence of iron sulfate in the PEO electrolyte on titanium causes a change in color to yellow and red [7]. Considering the application of corrosion inhibitors as electrolyte additives in other conversion coating processes such as anodizing [8,9], their use in PEO process has also recently attracted attentions. Oleinik et al. [10] investigated the effect of corrosion inhibitors in PEO process on aluminum-based alloys. They reported that existence of corrosion inhibitors raised hydrophobization. Another major advantage of PEO coating process in comparison with other conversion coatings such as anodizing is that the former is environmentally friendly [11,12]. Hence, it can attract more attention to employ non-toxic materials such as eco-friendly corrosion inhibitors as additives to the electrolyte to improve corrosion and mechanical behavior of PEO coatings on titanium. Atenolol is an antihypertensive with a chemical formula of $C_{14}H_{22}N_2O_3$ with a molecular weight of 266 g/mol [13]. The effect of atenolol as corrosion inhibitor was previously investigated. The results revealed that atenolol acts as an inhibitor against general corrosion and pitting in aluminum and Al—Si alloys in HCl media [14]. Accordingly, application of atenolol as a non-toxic additive to the electrolyte, which is readily accessible and inexpensive in PEO coating, on titanium surfaces may become a matter of considerable interest. Since atenolol is mainly used in medical and dental applications, it is necessary to use non-toxic materials in the coating process.

In addition, there are various methods to improve mechanical properties of PEO coatings on titanium including addition of hard ceramic nanoparticles suspended in an electrolyte [15], combination with other coating processes [16], application of new electrolyte compounds [17], performance of secondary heat treatments on the coatings [18], etc. The present work is conducted to investigate the effect of atenolol as an additive in the electrolyte (together with α-Al_2O_3 nanoparticles)

* Corresponding author.
E-mail addresses: maliofkh@gmail.com, khazraei@modares.ac.ir (M. Aliofkhazraei).

http://dx.doi.org/10.1016/j.surfcoat.2016.07.048
0257-8972/

on absorption of nanoparticles from the suspension, chemical structure, morphology and corrosion and mechanical behavior of properties of the oxide coatings obtained on commercially pure titanium (CP-Ti) surfaces through plasma electrolyte oxidation process.

2. Experimental procedure

2.1. PEO coating

CP-Ti sheets (ASTM-Grade 2) with dimensions of 50 mm × 50 mm × 1 mm were selected as the substrate material. Prior to the coating process, samples were polished until Ra < 1 μm, cleaned in acetone via ultrasonic, washed by deionized water and dried in warm air. The PEO process was carried out by means of a 20 kW DC power supply under the constant current density of 20 mA/cm^2 and for 12 min in an aqueous solution. In this process, the substrate (anode) is placed in a cell made of stainless steel (cathode) with a recirculating water cooling system. Since the effect of atenolol alone was to be considered in this project, the simplest electrolyte (single-component) was used. The electrolyte utilized in PEO process was composed of 8 g/L $Na_3PO_4 \cdot 12H_2O$ with/without 25 g/L α-Al_2O_3 nanoparticles and atenolol additive in deionized water. As shown in Fig. 1, the nanoparticles were analyzed by transmission electron microscopy (TEM; JEOL-2010). The average size of alumina nanoparticles was 22 nm. Several primary tests were carried out to acquire the concentration range of atenolol. It was observed that at concentrations higher than 4.5 g/L, sparks immediately reached a destructive state and the coating process would not be performed soundly. Thus, the maximum concentration of atenolol was set to be 4.5 g/L. To investigate the effect of atenolol additive, samples with atenolol concentrations of 0, 1.5, 3 and 4.5 g/L were provided. The denominated title for each sample is given in Table 1. The electrolyte temperature during the coating process was kept at 25 °C. All samples were washed with deionized water after the coating process and dried in warm air.

2.2. Characterization

Voltage variation during the sparking was automatically recorded by means of avomoter (digital multimeter; APPA 505). Samples were weighed before and after the coating (AND, GR-202, precision ± 50 μg balance). X-ray diffractometer (XRD, Philips; X'Pert MPD) working with Co Kα radiation (λ: 1.78897 Å) at a scanning rate of 0.02°/s was used for phase composition analysis. The elements distribution on surfaces and cross sections of the coatings were provided through energy dispersion X-ray spectroscopy (EDS; Oxford Instruments). The morphology of surfaces and cross sections was also studied by field emission scanning electron microscopy (SEM; Philips XL 30 and SIGMA/VP, Zeiss). The average size of alumina nanoparticles in the PEO suspensions with different concentration of atenolol after mechanical stirring for 24 h before use was determined by a dynamic light scattering spectroscopy (DLS; Zetasizer NanoZS, Malvern Instruments). Corrosion behavior of the coatings was evaluated by means of potentiodynamic polarization tests and electrochemical impedance spectrometry. Potentiodynamic polarization tests were carried out at a scan rate of 1 mV/s, from −300 to +3000 mV with respect to the corrosion potential (E_{corr}) using an EG&G Model 273A. Also, electrochemical impedance spectroscopy (EIS; Solarton 1260) in the frequency range between 65-kHz and 10 mHz with an amplitude of ± 10 mV, was employed. Both electrochemical tests were carried out in Ringer's solution (8.6 g/l NaCl, 0.3 g/l KCl and 0.33 g/l $CaCl_2 \cdot 2H_2O$), at 37 ± 0.5 °C. In these procedures, standard calomel electrode (SCE) and platinum were used as a reference and auxiliary electrodes, respectively. A nanoindentation testing system (Nanoindentation Tester CSM) with a Berkovich diamond indenter was employed to measure mechanical properties of PEO coating. For this purpose, the samples were cut, mounted, and mechanically polished down to the average roughness of 0.02 μm. The maximum load and its loading and unloading rates were adjusted to be 3 mN and 6 mN/min, respectively. Load–displacement curves were recorded and elastic recovery was calculated. Hardness and elastic modulus were determined using the Oliver and Pharr method [19]. In order to study the wear resistance of the coatings, the pin-on-disk test method was employed where the pin was 40 mm in length and 5 mm in diameter. The disk was a composite made of polymer in matrix and SiC as reinforcing particles. The normal load was 24 N, angular velocity was 50 rpm and wear distance for specimens with and without nanoparticles was 200 and 50 m, respectively.

Table 1
Samples code in different phosphate based electrolytes.

	Sample code							
Electrolyte components	A0	A1.5	A3	A4.5	AA0	AA1.5	AA3	AA4.5
Atenolol (g/L)	0	1.5	3	4.5	0	1.5	3	4.5
Alumina (g/L)	0	0	0	0	25	25	25	25

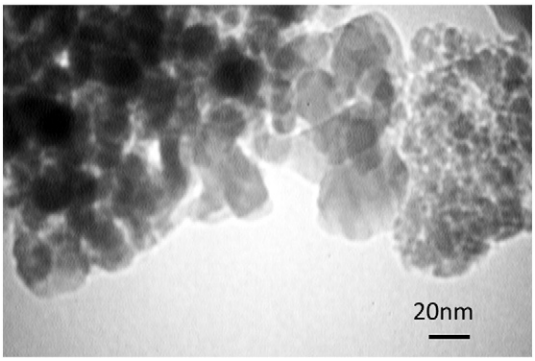

Fig. 1. TEM micrographs of alumina nanoparticles.

3. Results and discussion

3.1. Voltage-time curves

The voltage-time curves of the PEO coating process during sparking under constant current density for the coated samples at different electrolytes are plotted in Fig. 2. The voltage-time plot shows the effect of atenolol addition to the phosphate-based electrolyte and suspension. As shown in this figure, sparking during the PEO process occurred at lower potential ranges in the electrolyte compared with the suspension. The current density was kept constant; then, an increase in sparking voltage implies an increase in resistance of the system. Considering

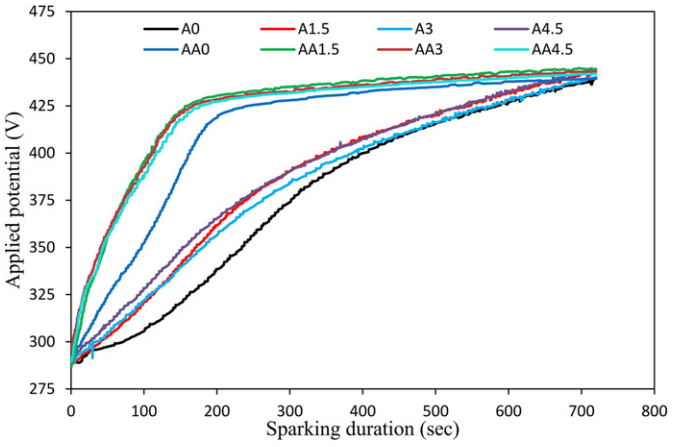

Fig. 2. The voltage-time curves of the PEO process during sparking under constant current density of 20 mA/cm^2 for 12 min on the coated samples at different electrolytes.

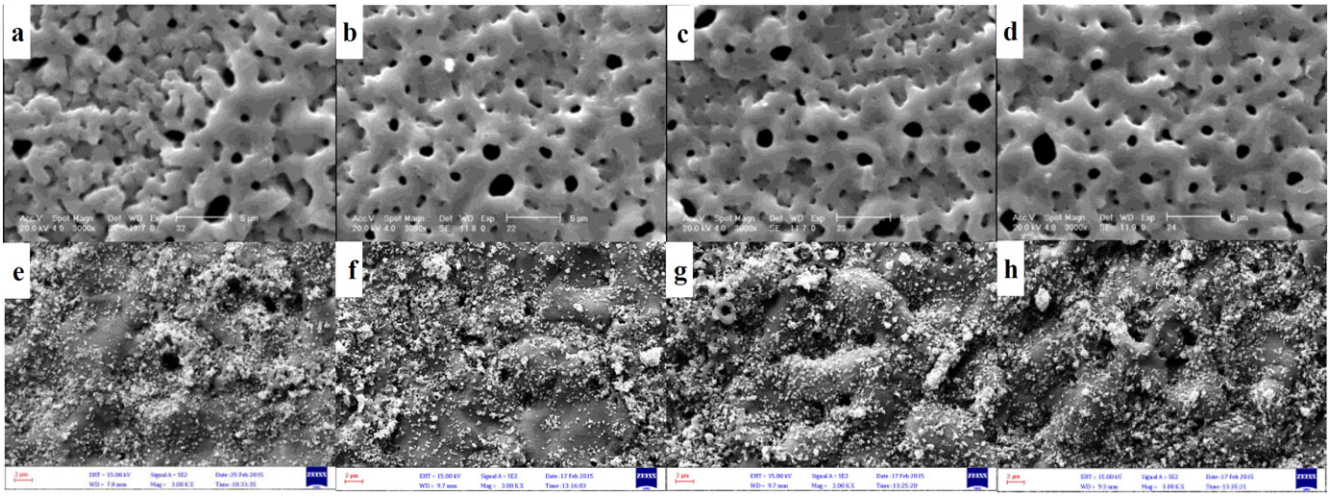

Fig. 3. SEM micrographs of the surfaces of coated samples in the electrolyte containing different concentrations of atenolol with/without alumina nanoparticles: a)A0, b)A1.5, c)A3, d)A4.5, e)AA0, f)AA1.5, g)AA3 and h)AA4.5.

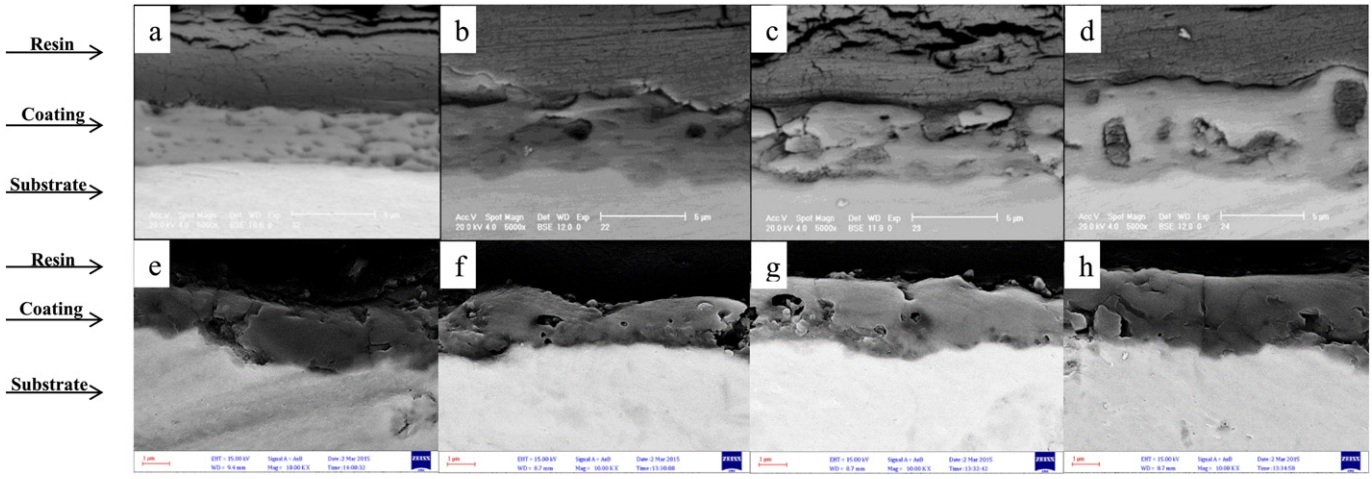

Fig. 4. SEM micrographs of the cross sections of coated samples in the electrolyte containing different concentrations of atenolol with/without alumina nanoparticles: a)A0, b)A1.5, c)A3, d) A4.5, e)AA0, f)AA1.5, g)AA3 and h)AA4.5.

the fact that resistance of the electrolyte is unchanged, the system resistance might be attributed to the coating. Therefore, an increase in the coating resistance may be due to the existence of alumina nanoparticles. It is possible to divide potential variations based on sparking time during the coating process into two separate steps. The two-step nature of voltage-time plots roots from the fact that current density generally consists of electron current density and ion current density where the former is not dependent on film resistance while the latter is its function [20]. Within the first step that potential variations increase dramatically and ionic current density mainly constitutes the overall current density. Hence, voltage is required to increase so that the current is maintained constant with film growth. This stage is named as spark anodizing through which a large number of small size sparks are observed as the white light rapidly scanning the electrode surface. However, in the second step, the overall current density is almost equal to electron current density which is independent of the oxide film resistance; therefore, the voltage remains constant. In this stage, steady state sparking is established in which separate orange sparks move slowly on the electrode surface. Thus, it can be stated that atenolol causes an increase in coating resistance at both conditions (with and without alumina nanoparticles).

Table 2
Weight variations percentage, thickness, average diameter of surface pores, and surface and cross-section porosity percentage of the coated samples in different electrolytes.

Sample code	Weight variations percentage			Thickness (μm)	Surface porosity percentage	Cross section porosity percentage	Surface pores diameter average (μm)
	$m_{1\ (g)}$	$m_{2\ (g)}$	$(\frac{m_2-m_1}{m_1}) \times 100$				
A0	6.8361	6.8446	0.12	2.5	7.8	9.5	1.6
A1.5	7.0123	7.0232	0.15	3.6	6.2	6.9	1.4
A3	6.9926	7.0046	0.17	3	7.3	15.2	1.5
A4.5	6.9571	6.9799	0.33	4.6	8.2	14.0	1.5
AA0	7.1231	7.1389	0.22	2	2.0	10.2	1.6
AA1.5	6.9000	6.9154	0.22	1.6	2.0	8.2	1.1
AA3	6.8397	6.8597	0.29	2.1	4.9	6.5	1.0
AA4.5	7.0093	7.0288	0.28	2.5	4.0	8.3	1.6

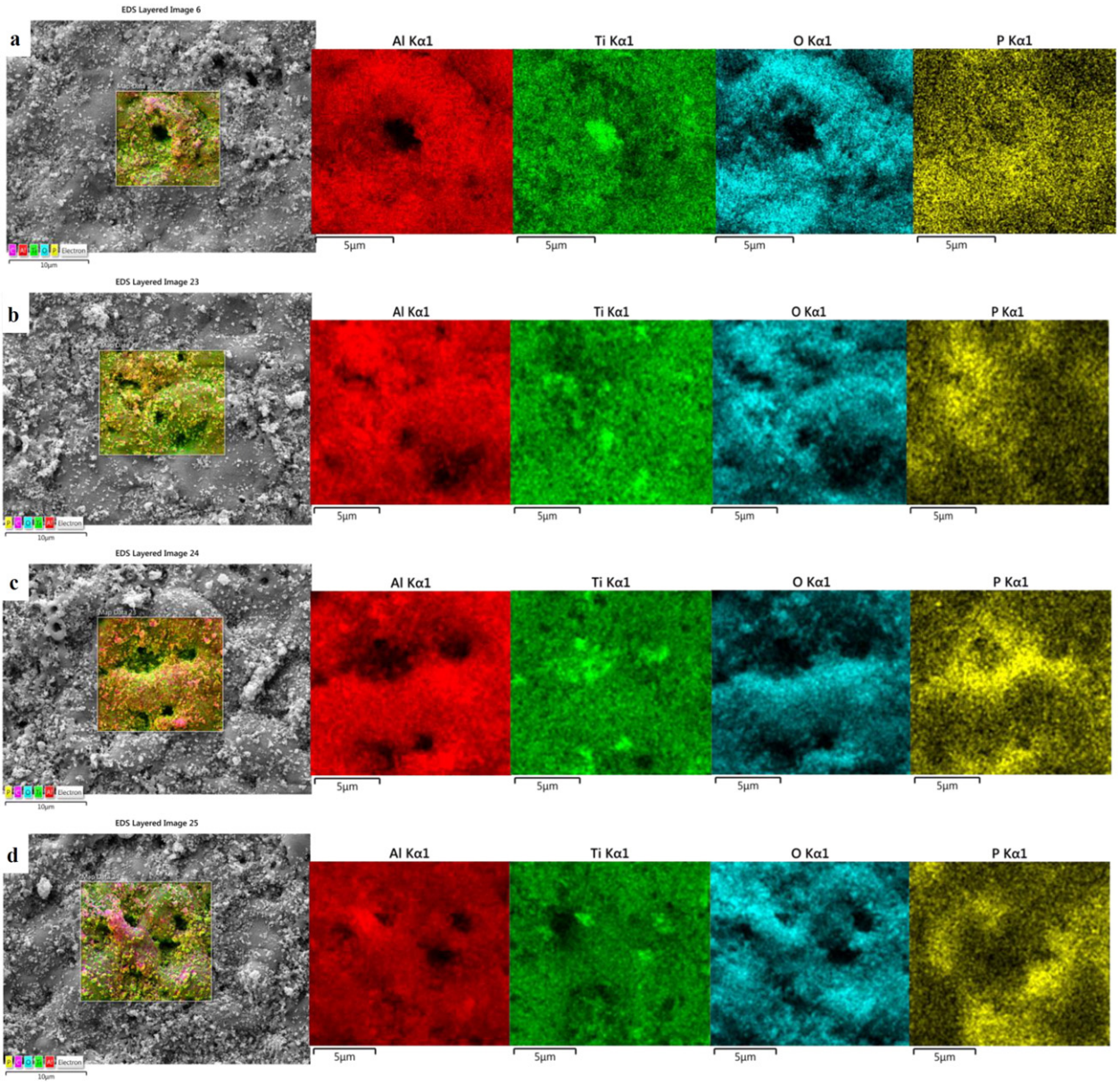

Fig. 5. Elemental distribution maps of PEO coating surface in alumina suspension containing different concentrations of atenolol; a)AA0, b)AA1.5, c)AA3 and d)AA4.5.

3.2. Microstructure and composition

3.2.1. SEM results of PEO coatings

SEM micrographs of the surfaces and cross-sections of coated samples in the electrolyte containing different concentrations of atenolol with/without alumina nanoparticles are illustrated in Figs. 3 and 4. Weight variations percentage caused by the PEO coating is presented in Table 2. Moreover, thickness, average diameter of surface pores, and surface and cross-section porosity percentage of the coated samples in different electrolytes were calculated by jMicroVision 1.2.7 image analysis software (Table 2). Weight variations of all samples showed a positive trend implying that the amount of materials participated in coating formation was higher than the amount of substrate dissolved. Regarding the effect of atenolol in weight changes, it was observed that the increase in atenolol concentration in no-alumina electrolyte caused weight changes to reach 0.33; however, when adding alumina nanoparticles to the electrolyte, no significant weight change was recorded.

On the basis of the results obtained from SEM micrographs of surfaces and cross sections (Table 2), one may come to the conclusion that all coatings had porous structures and there were micro-pores uniformly covering the surface of coatings. Formation of such pores is due to the evolution of gas from molten materials caused by coating growth processes. These pores allegedly would not penetrate through the whole thickness of the oxide layer [21]. Molten products around

Table 3
EDS results of PEO coating surface in alumina nanoparticles suspension containing different concentrations of atenolol.

	Element (wt.%)			
Sample code	Ti	Al	O	P
AA0	39.49	31.32	26.24	2.95
AA1.5	41.26	28.96	26.35	3.43
AA3	40.84	29.75	25.55	3.86
AA4.5	35.86	31.67	28.71	3.67

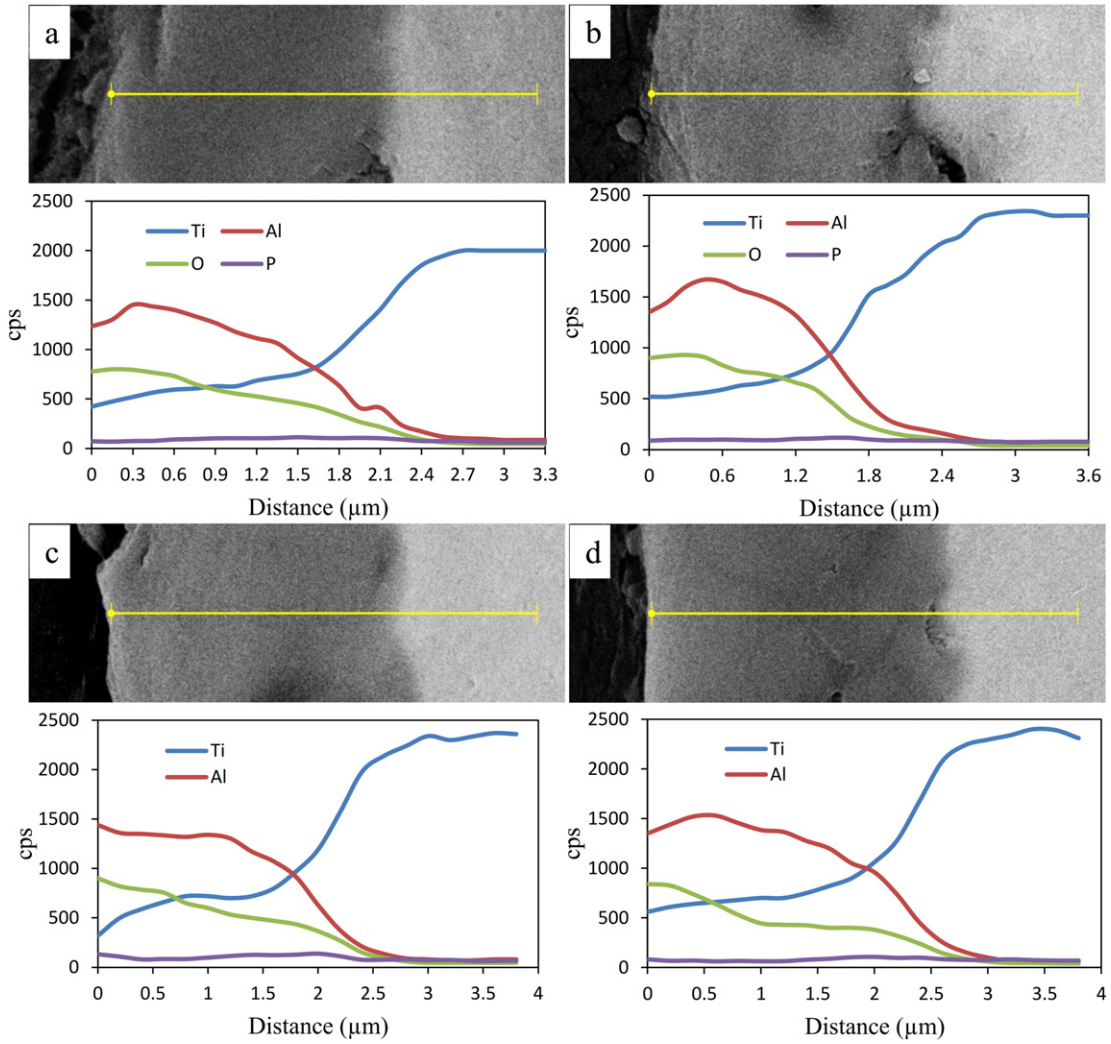

Fig. 6. Linear elemental distribution of PEO coating cross section in alumina suspension containing different concentrations of atenolol; a)AA0, b)AA1.5, c)AA3 and d)AA4.5.

volcanic pores reveal the fact that the plasma temperature during the process would be incredibly high (2300–3000 °C) [22]. As it may be observed, the addition of nanoparticle led to the closure of many porosities and the porosity percentage in the surface is reduced. The porous structure of coatings with no nanoparticles was approximately similar and the pores content did not significantly vary with concentration of atenolol. In the case of applying no alumina, porosity percentage and the average diameter of surface pores were almost constant. However, with the addition of alumina to the electrolyte, the average diameter of surface pores still remained constant while porosity percentage of the coating surface was decreased >50% compared with coatings without nanoparticles. Moreover, with the increased concentrations of atenolol in no-alumina electrolyte, porosity percentage of the cross section, on the contrary to the surface, was increased by 50%. It is worth mentioning that porosity percentage of cross sections in samples coated in the electrolyte containing alumina was less than that produced in no-alumina electrolyte, probably due to the pores being filled by alumina nanoparticles [23]. In addition, the coating surface at lower atenolol concentrations in the electrolyte contains alumina (Fig. 3 (e) and (f)) was rather smooth while at higher concentrations (Fig. (g) and (h)) the coating surface seemed to be rough probably due to absorption of nanoparticles in walls and volcanic pores, as well as a coarser volcanic structure by deposition of molten oxide. The existence of coarser volcanic structures means the creation of larger sparks and emission of more molten oxide from the area of sparking [24]. The increase in additive concentration in the electrolytes with/without alumina had no considerable effect on the diameter of pores on the coating surface. In fact, the diameter of melt discharge channel did not change at different additive concentrations. However, when adding alumina nanoparticles to the electrolyte, the amount of molten oxide discharging through the channel was increased at higher concentrations of atenolol. Considering the fact that diameter of the discharge channel was unchanged despite the amount of discharging molten oxide being increased, it may be concluded that sparking durations lingered. Longer durations of sparking could be effective in absorption of nanoparticles when its mechanism is based on impact between nanoparticles and the molten oxide.

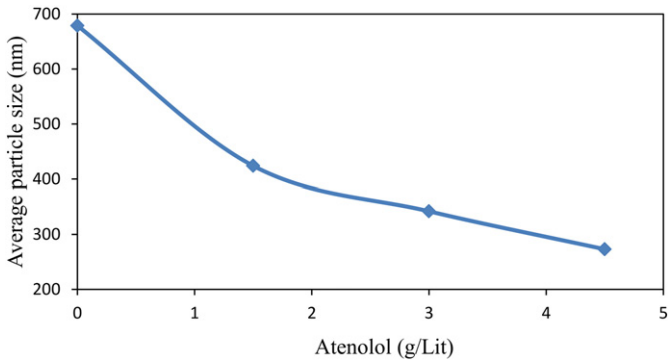

Fig. 7. Alumina particle size average in alumina suspension against atenolol concentration.

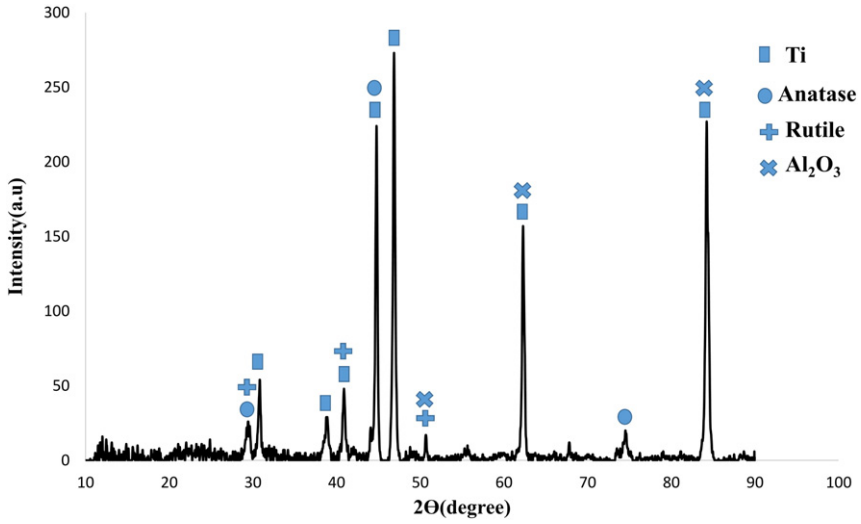

Fig. 8. XRD pattern of AA4.5 sample.

SEM micrographs of cross-sections (Fig. 4) revealed that with an increase in atenolol concentration from zero to 4.5 g/L, coatings produced in no-alumina electrolyte became greatly thicker. According to results of image analysis in Table 2, an increase in additive concentration with no alumina caused thickness to raise twice; while, in the case of presence of alumina, no significant increase was observed. Also, coating/substrate interface in all samples coated in the electrolytes with/without alumina was thoroughly continuous and free of cracks. Due to the nature of the formed oxide layer, a porous structure was developed. However, porosity within the coating apparently increased at higher concentrations of atenolol in the no-alumina electrolyte. In the case of presence of alumina, the coating was seen to become less porous toward the inside of the coating which is due to filling of the pores by alumina nanoparticles.

3.2.2. Chemical compositions of PEO coatings

Elemental distribution maps of samples surfaces coated in alumina nanoparticles suspension containing different concentrations of atenolol are shown in Fig. 5. The result of elemental distribution analysis on surfaces of samples coated in alumina nanoparticles suspension containing different concentrations of atenolol is given in Table 3. Because the aim of this work is to study the effect of atenolol addition on the absorption of alumina nanoparticles from the suspension during the coating process, elemental distribution analysis was only carried out on surfaces of samples coated in alumina-bearing suspension. Aluminum content was high all over the surface, implying the substantial absorption of this element from the suspension PEO coating process in comparison with other coating methods. However, the existence of atenolol or its concentration did play a meaningful role in alumina absorption level. Similar to aluminum, titanium content was also not changed along the elemental distribution map; except that more titanium was detected around surface pores probably due to the low thickness of the coatings and interference of titanium substrate. Contents of other elements (oxygen and phosphorous) did not vary with the introduction of atenolol to the suspension. On this ground, the elemental distribution changes through the thickness of coatings by means of linear elemental distribution of coating cross section were investigated.

Fig. 6 shows the linear elemental distribution of PEO coating cross section in alumina nanoparticles suspension containing different concentrations of atenolol. Distribution changes in titanium, oxygen and phosphorous within the cross sections of all samples approximately followed similar trends. Phosphorous content did not change throughout the cross sections. Oxygen content was lessened toward inner areas of coatings unanimously in all samples and ultimately titanium content was improved beneath the surfaces. Contrarily, aluminum content within the coatings cross sections varied with the addition of atenolol to the suspension indicating that alumina absorption is affected by

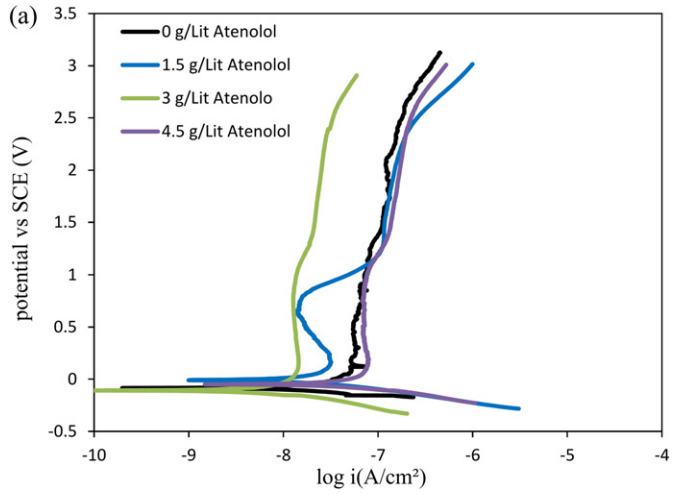

Fig. 9. The potentiodynamic polarization curves of coating obtained at different concentration of atenolol without alumina nanoparticles.

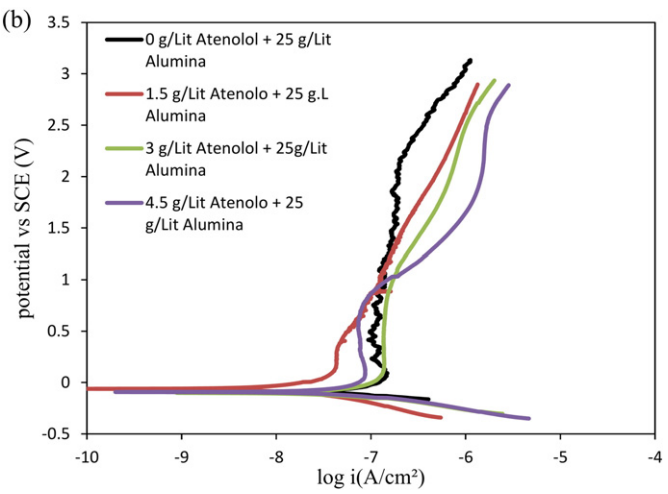

Fig. 10. The potentiodynamic polarization curves of coating obtained at different concentration of atenolol with alumina nanoparticles.

Table 4
Parameters obtained from the polarization curves.

Parameters	Sample code							
	A0	A1.5	A3	A4.5	AA0	AA1.5	AA3	AA4.5
E_{corr} (mV)	−78.5	−6.9	−112	−48	−91.7	−51	−108	−91
i_{corr} (nA/cm2)	11.0	9.6	3.8	22.2	37.9	6.9	26.7	28.1

the concentration of atenolol in the alumina nanoparticles suspension. At lower atenolol concentrations (Fig. 6 (a) and (b)), aluminum content was constant within a small depth of the coating (maximum depth of 1 μm from the surface) and then decreased to zero. In comparison, at higher concentrations of atenolol (Fig. 6 (c) and (d)) aluminum content was constant within a relatively large depth of the coating (about 2 μm) near the interface. Therefore, unlike the EDS results obtained from the coatings surfaces, an increase in atenolol concentrations in the suspension led to some changes in nanoparticles distribution trends along with the thickness of coatings. In other words, an increase in additive concentration caused a higher level of alumina nanoparticles absorption. The existence of atenolol in the electrolyte, acting as a surfactant material, leads to an increasing distribution of particles throughout the electrolyte and prevents agglomeration effect. In order to measure average size of alumina particle in the suspension, dynamic light scattering test was employed. The average alumina particle size in alumina suspension with atenolol concentration is plotted in Fig. 7. The introduction of atenolol and further increasing its concentration led to formation of finer particles. The finer particles are, the more absorption of alumina nanoparticles occurs during the coating process.

3.2.3. Phase analysis of PEO coating

XRD pattern of AA4.5 sample shows the presence of Al_2O_3, Ti, rutile, and anatase phase (Fig. 8). Ti phase originated from the substrate due to the low thickness and porous structure of PEO coating. Presence of Ti phase in the XRD pattern in PEO coating also has been reported in other report [17]. Al_2O_3 phase originated from Al_2O_3 nanoparticle which is suspended in the electrolyte. Sarbishei et al. [25] also indicated the presence of Al_2O_3 phase during the PEO coating in the electrolyte containing Al_2O_3 nanoparticle. The presence of Al_2O_3 in the coating is the indicative of nanoparticle absorption during coating treatment. Rutile and anatase phase are originated from the oxide layer fabricated during PEO coating reported by other researchers [26,27].

3.3. Corrosion behavior

3.3.1. Potentiodynamic polarization

Corrosion behavior of coating fabricated at different conditions was characterized using potentiodynamic polarization test. The potentiodynamic polarization curves of the coating obtained at different concentrations of atenolol without and with alumina nanoparticle are represented in Figs. 9 and 10, respectively. Corrosion potentials (E_{corr}) and corrosion current densities (i_{corr}) are obtained from the potentiodynamic curves (Table 4).

As can be seen in the potentiodynamic curves, the atenolol concentration can affect the corrosion resistance of coating. Generally, the oxide film formed on the surface improves corrosion resistance by limiting absorption of corrosive ions and hence reducing charge transfer over the metal-electrolyte interface [17]. The level of corrosion resistance depends on oxide film properties such as chemical composition, thickness, defect structures, and composition of the corrosive medium [28]. As can be seen in the polarization curves, the corrosion resistance of the coating is improved by adding atenolol in the electrolyte and A3 samples have the best corrosion resistance. Thickness and compactness of coating are among the main factors affecting the corrosion resistance of the coating. It was previously revealed that thickness was increased at higher concentrations of atenolol which would lead to corrosion resistance improvement. However, there were some pores on the surface of A4.5 which result in corrosive species penetration into the substrate leading to deterioration of corrosion resistance in this sample. In the case of coatings containing alumina nanoparticle, by increased concentrations of atenolol, absorption of nanoparticles occurred much more toward the surface which filled the pores. Filling of surface pores led to the uniformity of surface [29] and less roughness. Filling of pores and reduction surface roughness refrain corrosive ions from entering into the coating toward the substrate which in turn leads to corrosion

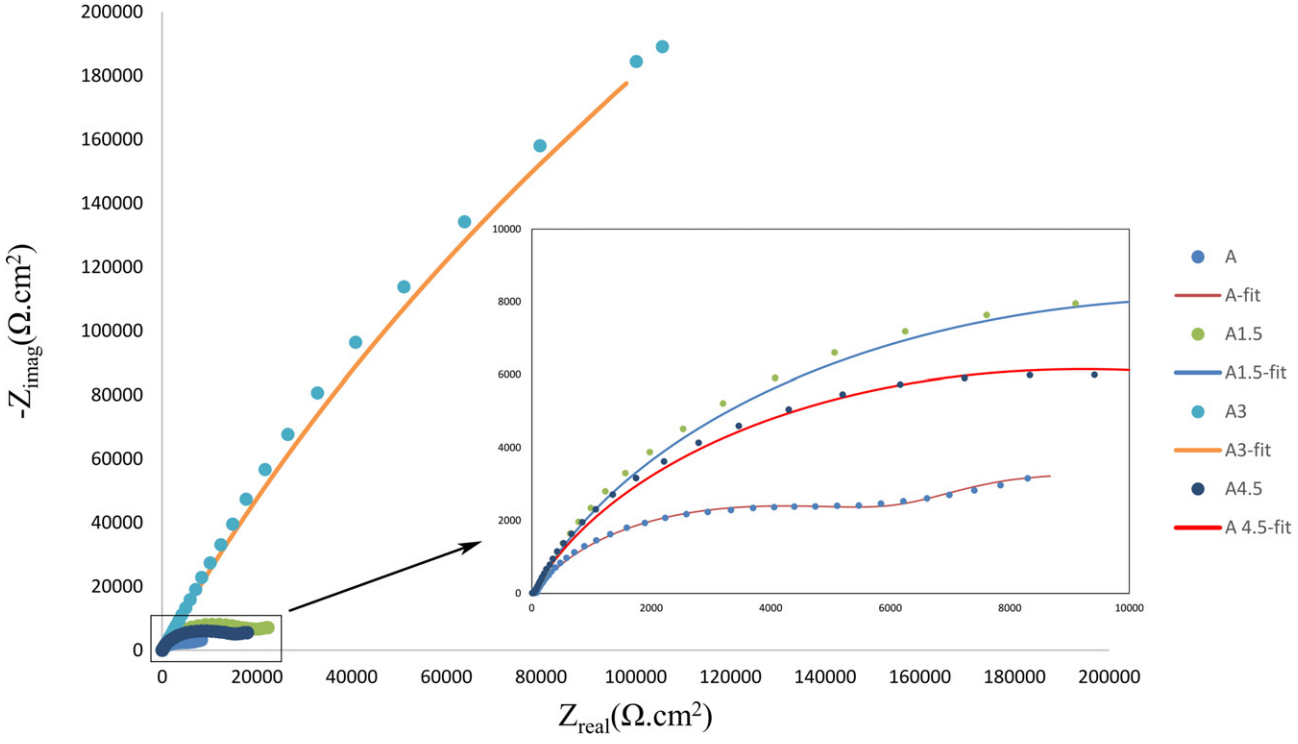

Fig. 11. Nyquist plot of samples coated in electrolyte without alumina and different concentrations of atenolol.

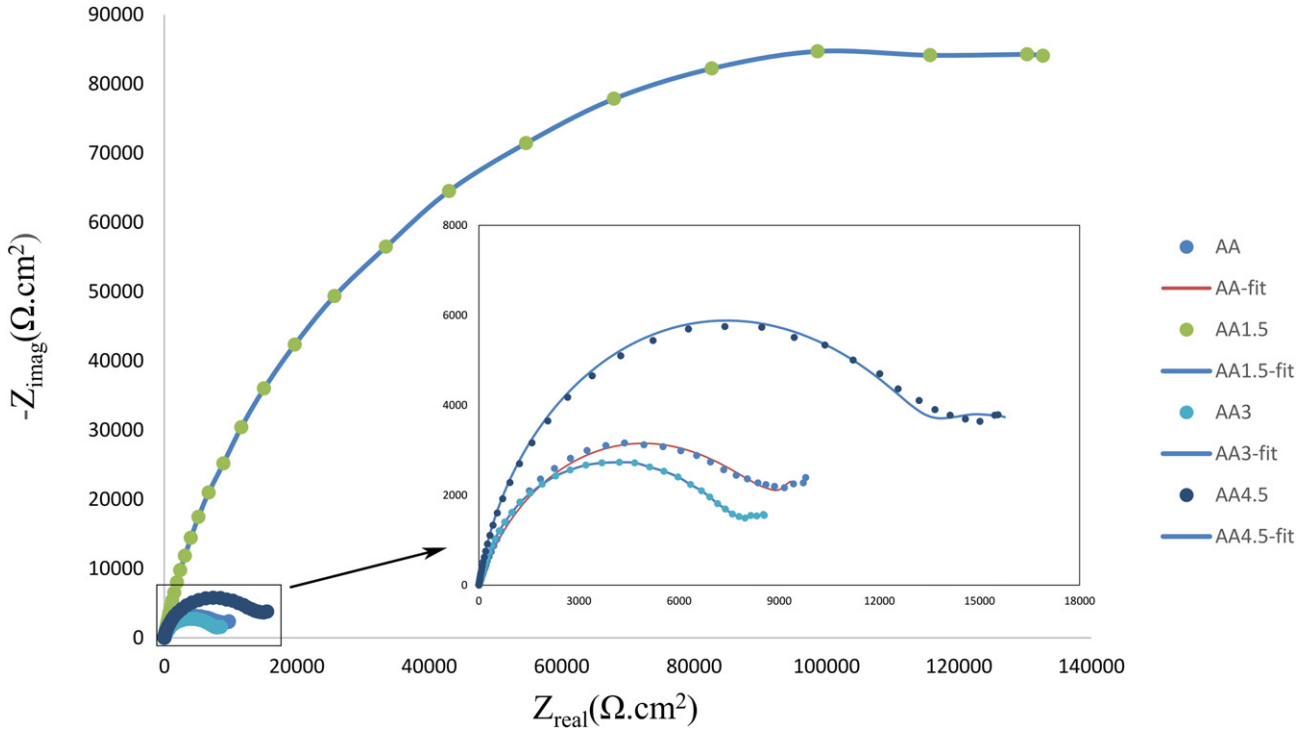

Fig. 12. Nyquist plot of samples coated in alumina suspension with different concentrations of atenolol.

resistance improvement [30]. As it is seen, the E_{corr} of all samples is almost the same, implying the same chemical stability of all coating.

3.3.2. Electrochemical impedance spectroscopy

Electrochemical impedance spectroscopy was carried out on the specimens in order to study the corrosion behavior of the coatings in more details and validate the results of polarization tests. Nyquist plots of specimens coated in the electrolytes containing a different concentration of atenolol without and with alumina nanoparticle are illustrated in Figs. 11 and 12 respectively. Since it is the most similar to EIS data, the equivalent circuit showed in Fig. 13 was used to analyze impedance plots. In the equivalent plot, R_s is solution resistance. The PEO coating has mainly two layers consisting barrier layer and a porous layer. Thus, in the equivalent circuit, R_1 is the porous layer resistance and R2 is the barrier layer resistance. The proposed electrical equivalent circuit model consisted of constant phase element in parallel with porous layer resistance (CPE1) and also CPE2 in parallel with barrier layer resistance. Also, the W shown in the equivalent circuit is Warburg diffusion coefficient. Constant phase element (which is a broader concept) was used instead of a capacitor. Application of constant phase element not only reduces the probability of systematic error also provides more information about dielectric properties of coatings.

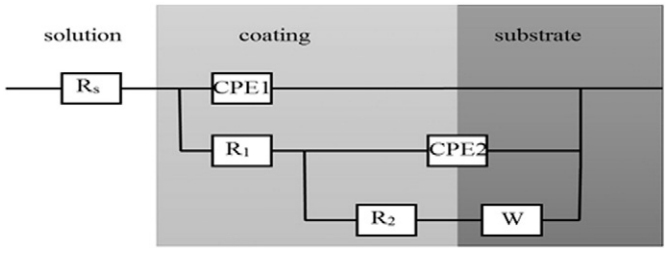

Fig. 13. Equivalent circuit fitted with EIS data.

The impedance function of constant phase element is defined as follows [31]:

$$Z = \frac{(j\omega)^{-n}}{Y_0} \quad (1)$$

Where, Y_0 is admittance and n is constant, 0, 1, or −1 according to which CPE would show pure inductive, resistive, or capacitive behavior, respectively. The presence of Warburg coefficient in the equivalent circuit of the coating impedance behavior indicates that corrosion behavior of the oxide coating is under diffusion control. On this occasion, the overall reaction rate could be controlled by diffusion of corrosive ions, explaining why Warburg coefficient is introduced to the equivalent circuit. The calculated circuit elements are presented in Table 5. In no-alumina coatings (A0, A1.5, A3, and A4.5), an increase in atenolol concentration by 3 g/L in the electrolyte led to increasing in polarization resistance. Further increasing of atenolol concentration (up to 4.5 g/L) reduced charge transfer resistance. Thus, it can be concluded that by the addition of atenolol by 3 g/L to the electrolyte, corrosion resistance could be improved that is shown in n value of impedance data. As it is mentioned in the polarization section, AA1.5 have the best corrosion resistance in the electrolyte containing alumina nanoparticle which also

Table 5
Results of EIS curves in different electrolytes.

Sample code	$R_{soultion}$ (Ω cm^2)	$CPE_{coating}$ (10^{-6} F)	$n_{Coating}$	$R_{Coating}$ (Ω cm^2)	CPE_{dl} (10^{-6} F)	n_{dl}	R_{Ct} (Ω cm^2)
A0	40.7	0.2	0.90	17.3	101.0	0.76	5978
A1.5	56.6	104.0	0.75	2.1 E-5	59.2	0.60	9348
A3	12.8	1.2	0.77	6.8	27.2	0.76	1.33 E6
A4.5	5.4	2.8	0.74	29.7	48.9	0.81	21,300
AA0	7.7	83.0	0.74	32.0	7.3	0.61	9559
AA1.5	20.2	6.6	0.99	1.8	29.0	0.83	211,420
AA3	8.4	10.0	0.92	19.9	48.8	0.80	6931
AA4.5	5.1	60,440	0.88	42.0	4.5	0.43	14,414

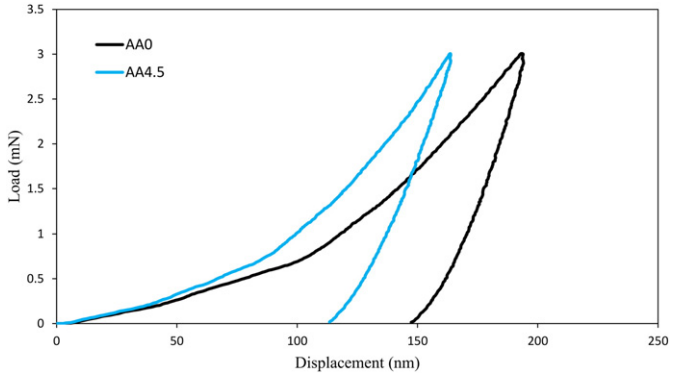

Fig. 14. Load-displacement curves of AA0 and AA4.5 samples.

Table 6
Obtained results from load-displacement curves (Fig. 14).

Samples code	Hardness (GPa)	Elastic module (GPa)	H/E	Elastic recovery (%)
AA0	4.5	106.4	0.042	16
AA4.5	8.0	117.6	0.068	25

appears in the impedance data. One of the factors affecting the corrosion resistance of the coating is roughness of coating that appears in the n parameter of impedance data. It may be observed that n value in the AA1.5 sample is about 1, implying the reduction of surface roughness and improvement of corrosion resistance.

3.4. Mechanical behavior

3.4.1. Nano-indentation test

In order to study the mechanical properties of coatings formed in the suspension with different concentrations of atenolol and determine their hardness and elastic modulus values, nanoindentation test was used. The coatings surfaces were polished to remove the adsorbed Al_2O_3 nanoparticles and reduce roughness and surface porosity. Fig. 14 shows load-displacement curves for AA0 and AA4.5 samples. The maximum load was 3 mN and loading and unloading rates were 6 mN/min so that both loading and unloading curves were non-linear. The maximum displacement at the 3 mN peak load for AA4.5 was less than that of AA0. Maximum displacements including elastic and plastic deformations occurred during loading while the elastic recovery occurred during unloading. According to Table 6, most of the displacement at load peak for AA4.5 is elastic recovery during unloading which equals 25% of the maximum displacement; while, elastic recovery of AA0 is only 16%. The increased proportion of elastic recovery in maximum displacement could mean an improvement in hardness and elastic modulus [32]. Results presented in Table 6 reveal that presence of atenolol in the PEO coating suspension leads to fairly improved hardness and elastic modulus. Based on other studies [15,29], the addition of reinforcing nanoparticles with proper mechanical properties within a softer matrix could noticeably improve mechanical properties of the produced composite. According to the results obtained in this work, an increase in atenolol concentration in the suspension of alumina nanoparticles from 0 in AA0 to 4.5 g/L in AA4.5, absorption of reinforcing nanoparticles within the nanocomposite coating structure was increased and consequently mechanical properties including hardness were improved.

3.4.2. Wear behavior

Wear behavior of PEO coatings including friction coefficient and wear rate was studied by means of a pin-on-disk wear test. The friction coefficient of coatings formed in different electrolytes is shown in Fig. 15. In the case of coatings formed in no-alumina electrolytes (Fig. 15 (a)), the presence of atenolol led to a lower friction coefficient compared with those coated in no-atenolol (A0) electrolyte. The least value of friction coefficient was 0.22 obtained from 4.5 g/L electrolyte. The data presented in Table 2 reveal that presence of atenolol increased the thickness of coatings. Adhesion strength of coatings increases

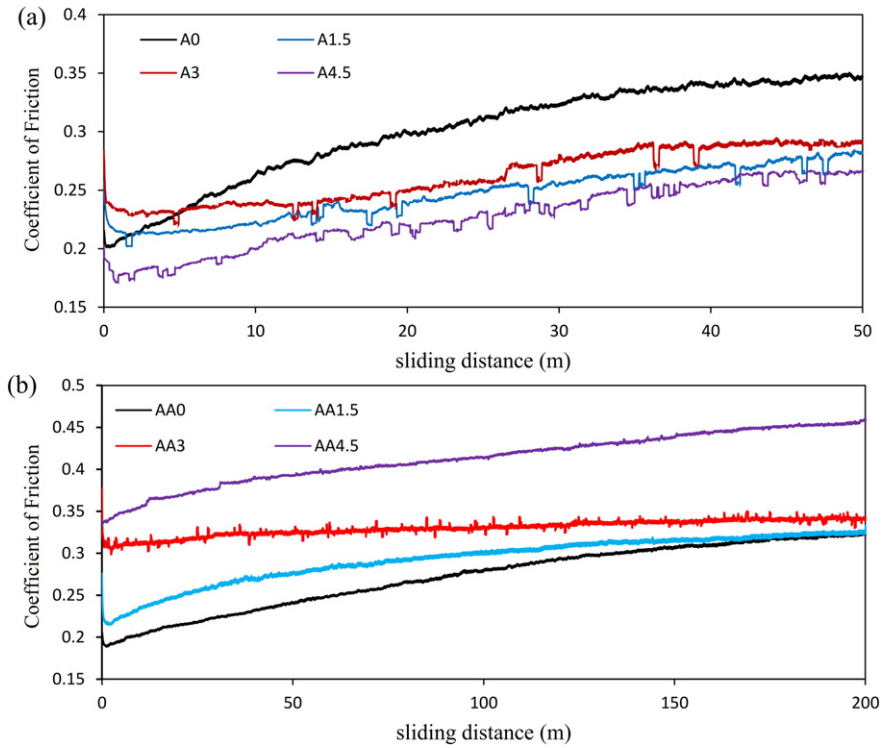

Fig. 15. Friction coefficient versus of PEO coated samples in different electrolytes: a) electrolytes without alumina and different concentrations of atenolol and b) alumina suspension with different concentrations of atenolol.

straightly with their thickness [33,34]. This increases, in turns, prevents coating removal and formation of released particles which fill the pores among SiC particles over the counterpart. Consequently, the contact area between counterpart and the specimen would not increase, explaining the less increase in friction coefficient [35]. However, PEO-coated in alumina suspension and various concentrations of atenolol were in different conditions (Fig. 15 (b)). By increased concentration of atenolol in the alumina suspension, the coated specimens were observed with significantly higher friction coefficient values compared with those coated in the no-atenolol suspension (AA0). The most value of friction coefficient was 0.41 obtained from 4.5 g/L atenolol concentration. As linear elemental distribution (Fig. 6), the existence of aluminum in the coating (implying alumina), is raised by the increase in atenolol concentration. The existence of alumina nanoparticles is probably effective in friction coefficient variations. In fact, these particles would release from the coating structure during the wearing and intensify plowing together with SiC particles on the counterpart increasing the coefficient friction.

Fig. 16 shows SEM micrographs regarding wear tracks of coated samples in different electrolytes. Micrograph of wear tracks of the sample coated in the no-atenolol/alumina electrolyte (Fig. 16 (a)) shows that the coating was completely removed from the surface implying the slight resistance to wearing. The appended SEM micrograph at higher magnification shows no trace of porosity over PEO coatings,

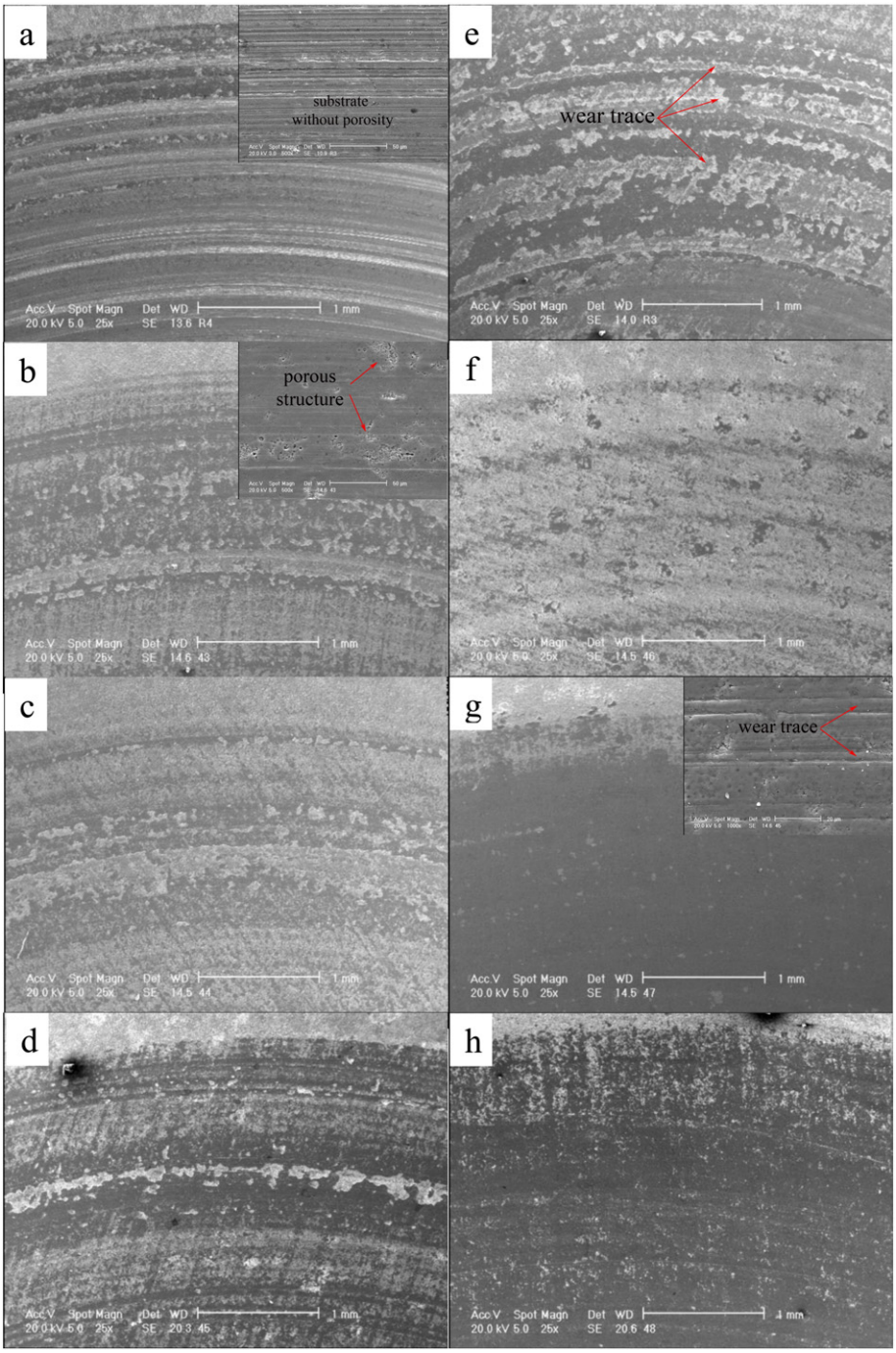

Fig. 16. SEM micrographs of wear tracks of samples coated in different electrolytes: a)A0, b)A1.5, c)A3, d)A4.5, e)AA0, f)AA1.5, gAA3 and g)AA4.5.

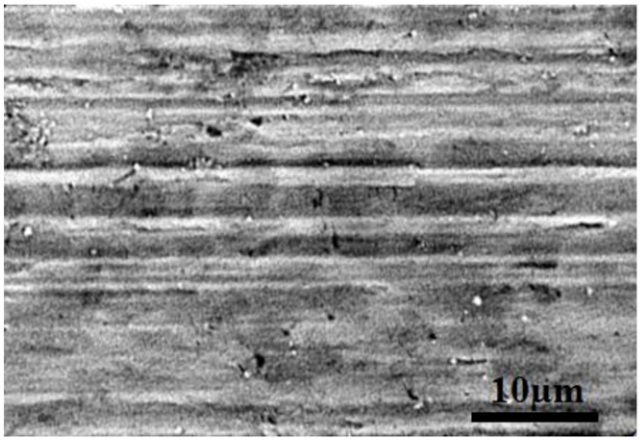

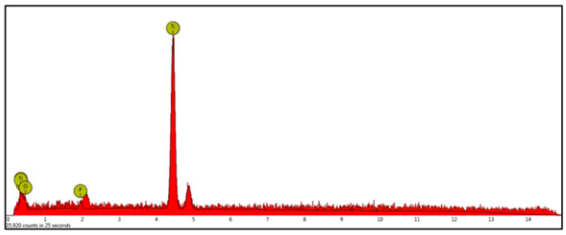

Element	Ti	O	P
Concentration (wt%)	70.5	28.0	1.5

Fig. 17. EDS result of worn surface of A0 sample.

indicating the complete removal of coatings [36]. In order to achieve certainty, elemental distribution spectrometry was employed over the worn surface (Fig. 17). Titanium content over the wear surface was approximately 70 wt.% that makes removal of the coating clear. However, wear resistance of coated samples was improved by the addition of atenolol and thickening coatings (Fig. 16 (b), (c) and (d)). Porosity over the appended micrograph (with higher magnification) demonstrates that wear did not reach the substrate during the wearing process [36]. According to the micrographs, the wear surfaces are not seen to have deep and broad tracks likewise the sample coated in the no-atenolol/alumina electrolyte (Fig. 16 (a)). Micrographs of wear tracks of PEO coating formed in alumina suspension and different concentrations of atenolol (Fig. 16 (e), (f), (g) and (h)) prove the significant role of atenolol additives in the improvement of wear resistance. There were deeper and broader tracks over the worn surface of the sample coated in no-additive electrolyte (Fig. 16 (e)) than others (Fig. 16 (f), (g) and (h)). These tracks imply the low wear resistance of coating [37], which is further provide by deep and broad wear tracks throughout the worn surface observed in appended micrograph (Fig. 16 (e)). Contrarily, PEO coating formed in atenolol containing suspension had smooth and polished worn surfaces with no trace of deep wear tracks. Appended micrograph (Fig. 16 (g)) reveal several tracks of less depth and width compared with the specimen with no atenolol in these coating (particularly in areas with most porosity), indicating an improvement of wear resistance. In addition, the existence of pores over the wear track means that wear process did not reach the substrate [36, 37]. Wear mechanism in these coatings is abrasive because of the nature of ceramic coatings (with little plastic deformation ability) and condition of the used pin. This mechanism might be confirmed by continuous grooves throughout the wear track in SEM micrographs (Fig. 16) [17,38].

Average wear rate and thickness of PEO coating in different electrolytes are presented in Table 7. The addition of atenolol in PEO coating formed in no-alumina electrolyte led to a reduction of wear rate values; the least wear rate was 0.466 µg/N.m obtained from the specimen with 4.5 g/L atenolol (A4.5). In fact, wear rate of the PEO coatings formed in atenolol containing electrolyte (A1.5, A3, and A4.5) was a function of their thickness so that with an increase in thickness, the wear rate was reduced. The obtained results are in accordance with previous works [39]. However, in the case of PEO coatings formed in alumina suspension, by increase atenolol concentrations the wear rate was significantly diminished. The average wear rate of the AA4.5 specimen was approximately 130 times less than that of AA0. It was mentioned earlier that the increase in atenolol concentration causes the formation of thicker coatings and consequently a reduction of wear rate. Also, the existence of alumina nanoparticles as a hard reinforcing phase in the titania matrix leads to improvement of wear rate [15]. By the addition of atenolol to the alumina suspension, the aluminum content (alumina) within the coating was increased (Fig. 6). The presence of reinforcing alumina nanoparticles in the rather softer titania matrix improves mechanical properties and wear resistance. Furthermore, according to the results obtained from nanoindentation test, hardness to Young's modulus ratio of samples coated in atenolol containing suspension was extremely higher than that of coated in no- atenolol suspension. Leyland et al. showed that hardness to Young's modulus ratio of ceramics may be used as a reliable measure to compare wear behavior of different materials. The high hardness to Young's modulus ratio of ceramic coatings implies improved wear resistance [40] . The present work revealed that addition of atenolol in the coating electrolyte reduces the wear rate by increasing the hardness to Young's modulus ratio.

Table 7
Results of wear rate of PEO coated samples in different electrolytes.

	Sample code							
Parameters	A0	A1.5	A3	A4.5	AA0	AA1.5	AA3	AA4.5
Thickness (µm)	2.5	3.6	3.0	4.6	2.0	1.6	2.1	2.5
Wear rate (10^{-6} g/N.m)	2.033	0.650	0.800	0.466	0.788	0.158	0.014	0.006

4. Conclusions

In this study, the effect of atenolol on microstructure, corrosion behavior, and mechanical behavior of nanocomposite PEO coating were investigated. Results of this study indicated that, by adding atenolol in alumina suspension, nanoparticle absorption was increased and therefore the coating porosity was decreased so that coating with compact structure were obtained. The decrease in coating porosity leads to an improvement in corrosion resistance. Mechanical behavior of coating evaluated using nanoindentation and pin-on-disk tests and results indicated that by the addition of atenolol in PEO electrolyte the coating thickness and the rate of hardness to Young's modulus was increased, resulting in the improved wear resistance of the coating.

References

[1] M. Fazel, H.R. Salimijazi, M.A. Golozar, M.R. Garsivazjazi, A comparison of corrosion, tribocorrosion and electrochemical impedance properties of pure Ti and Ti6Al4V alloy treated by micro-arc oxidation process, Appl. Surf. Sci. 324 (2015) 751–756.
[2] M. Aliofkhazraei, A. Sabour Rouhaghdam, T. Shahrabi, Abrasive wear behaviour of Si3N4/TiO2 nanocomposite coatings fabricated by plasma electrolytic oxidation, Surf. Coat. Technol. 205 (Supplement 1) (2010) S41–S46.
[3] X.L. Zhang, Z.H. Jiang, Z.P. Yao, Z.D. Wu, Electrochemical study of growth behaviour of plasma electrolytic oxidation coating on Ti6Al4V: effects of the additive, Corros. Sci. 52 (2010) 3465–3473.

[4] K.R. Shin, Y.G. Ko, D.H. Shin, Effect of electrolyte on surface properties of pure titanium coated by plasma electrolytic oxidation, J. Alloys Compd. 509 (Suppl) (2011) S478–S481.
[5] Y. HUANG, W. Yingjun, N. Chengyun, N. Kaihui, H. Yong, Preparation and properties of a cerium-containing hydroxyapatite coating on commercially pure titanium by micro-arc oxidation, Rare Metals 27 (2008) 257–260.
[6] M. Bayati, A. Moshfegh, F. Golestani-Fard, In situ growth of vanadia–titania nano/micro-porous layers with enhanced photocatalytic performance by micro-arc oxidation, Electrochim. Acta 55 (2010) 3093–3102.
[7] H. Tang, D.-z. Yu, F.-p. Wang, Y.-l. Wang, T.-z. Xin, J.-l. Xu, Influence of FeSO_4 concentration on color of films formed on titanium by micro-arc oxidation, Heat Treat. Met. 7 (2009) 006.
[8] V. Moutarlier, M. Gigandet, B. Normand, J. Pagetti, EIS characterisation of anodic films formed on 2024 aluminium alloy, in sulphuric acid containing molybdate or permanganate species, Corros. Sci. 47 (2005) 937–951.
[9] V. Moutarlier, M. Gigandet, J. Pagetti, L. Ricq, Molybdate/sulfuric acid anodising of 2024-aluminium alloy: influence of inhibitor concentration on film growth and on corrosion resistance, Surf. Coat. Technol. 173 (2003) 87–95.
[10] S. Oleinik, V. Rudnev, A.Y. Kuzenkov, T. Yarovaya, L. Trubetskaya, P. Nedozorov, Modification of plasma electrolytic coatings on aluminum alloys with corrosion inhibitors, Prot. Met. Phys. Chem. Surf. 49 (2013) 885–890.
[11] R.O. Hussein, X. Nie, D.O. Northwood, An investigation of ceramic coating growth mechanisms in plasma electrolytic oxidation (PEO) processing, Electrochim. Acta 112 (2013) 111–119.
[12] J.-H. Wang, J. Wang, Y. Lu, M.-H. Du, F.-Z. Han, Effects of single pulse energy on the properties of ceramic coating prepared by micro-arc oxidation on Ti alloy, Appl. Surf. Sci. 324 (2015) 405–413.
[13] G. Gece, Drugs: a review of promising novel corrosion inhibitors, Corros. Sci. 53 (2011) 3873–3898.
[14] M. Abdallah, I. Zaafarany, S. Al-Karanee, A.A. El-Fattah, Antihypertensive drugs as an inhibitors for corrosion of aluminum and aluminum silicon alloys in aqueous solutions, Arab. J. Chem. 5 (2012) 225–234.
[15] K. Kato, Wear in relation to friction — a review, Wear 241 (2000) 151–157.
[16] E. Arslan, Y. Totik, E.E. Demirci, I. Efeoglu, Wear and adhesion resistance of duplex coatings deposited on Ti6Al4V alloy using MAO and CFUBMS, Surf. Coat. Technol. 214 (2013) 1–7.
[17] A. Yerokhin, X. Nie, A. Leyland, A. Matthews, Characterisation of oxide films produced by plasma electrolytic oxidation of a Ti–6Al–4 V alloy, SuCT 130 (2000) 195–206.
[18] S. Cheng, D. Wei, Y. Zhou, Mechanical and corrosion resistance of hydrophilic sphene/titania composite coatings on titanium and deposition and release of cefazolin sodium/chitosan films, Appl. Surf. Sci. 257 (2011) 2657–2664.
[19] W.C. Oliver, G.M. Pharr, An improved technique for determining hardness and elastic modulus using load and displacement sensing indentation experiments, J. Mater. Res. 7 (1992) 1564–1583.
[20] L. Chang, Growth regularity of ceramic coating on magnesium alloy by plasma electrolytic oxidation, J. Alloys Compd. 468 (2009) 462–465.
[21] H. Guo, M. An, H. Huo, S. Xu, L. Wu, Microstructure characteristic of ceramic coatings fabricated on magnesium alloys by micro-arc oxidation in alkaline silicate solutions, Appl. Surf. Sci. 252 (2006) 7911–7916.
[22] A. Yerokhin, X. Nie, A. Leyland, A. Matthews, S. Dowey, Plasma electrolysis for surface engineering, Surf. Coat. Technol. 122 (1999) 73–93.
[23] T.S. Lim, H.S. Ryu, S.-H. Hong, Electrochemical corrosion properties of CeO 2-containing coatings on AZ31 magnesium alloys prepared by plasma electrolytic oxidation, Corros. Sci. 62 (2012) 104–111.
[24] S. Durdu, M. Usta, Characterization and mechanical properties of coatings on magnesium by micro arc oxidation, Appl. Surf. Sci. 261 (2012) 774–782.
[25] S. Sarbishei, M.A.F. Sani, M.R. Mohammadi, Study plasma electrolytic oxidation process and characterization of coatings formed in an alumina nanoparticle suspension, Vacuum 108 (2014) 12–19.
[26] Z. Yao, Z. Jiang, F. Wang, G. Hao, Oxidation behavior of ceramic coatings on Ti–6Al–4V by micro-plasma oxidation, J. Mater. Process. Technol. 190 (2007) 117–122.
[27] J.-H. Wang, J. Wang, Y. Lu, M.-H. Du, F.-Z. Han, Effects of single pulse energy on the properties of ceramic coating prepared by micro-arc oxidation on Ti alloy, ApSS 324 (2015) 405–413.
[28] M. Shokouhfar, C. Dehghanian, M. Montazeri, A. Baradaran, Preparation of ceramic coating on Ti substrate by plasma electrolytic oxidation in different electrolytes and evaluation of its corrosion resistance: part II, Appl. Surf. Sci. 258 (2012) 2416–2423.
[29] M. Aliofkhazraei, A.S. Rouhaghdam, Wear and coating removal mechanism of alumina/titania nanocomposite layer fabricated by plasma electrolysis, Surf. Coat. Technol. 205 (Suppl) (2011) S57–S62.
[30] M. Aliofkhazraei, R.S. Gharabagh, M. Teimouri, M. Ahmadzadeh, G.B. Darband, H. Hasannejad, Ceria embedded nanocomposite coating fabricated by plasma electrolytic oxidation on titanium, J. Alloys Compd. 685 (2016) 376–383.
[31] P. Zoltowski, On the electrical capacitance of interfaces exhibiting constant phase element behaviour, J. Electroanal. Chem. 443 (1998) 149–154.
[32] W. Xue, C. Wang, R. Chen, Z. Deng, Structure and properties characterization of ceramic coatings produced on Ti–6Al–4V alloy by microarc oxidation in aluminate solution, Mater. Lett. 52 (2002) 435–441.
[33] S. Durdu, S. Bayramoğlu, A. Demirtaş, M. Usta, A.H. Üçışık, Characterization of AZ31 Mg Alloy coated by plasma electrolytic oxidation, Vacuum 88 (2013) 130–133.
[34] S. Durdu, M. Usta, The tribological properties of bioceramic coatings produced on Ti6Al4V alloy by plasma electrolytic oxidation, Ceram. Int. 40 (2014) 3627–3635.
[35] I.M. Hutchings, Tribology: Friction and Wear of Engineering Materials(DOI) 1992.
[36] A. Yetim, Investigation of wear behavior of titanium oxide films, produced by anodic oxidation, on commercially pure titanium in vacuum conditions, Surf. Coat. Technol. 205 (2010) 1757–1763.
[37] D.S.R. Krishna, Y. Sun, Thermally oxidised rutile-TiO2 coating on stainless steel for tribological properties and corrosion resistance enhancement, Appl. Surf. Sci. 252 (2005) 1107–1116.
[38] H. Sharifi, M. Aliofkhazraei, G.B. Darband, A.S. Rouhaghdam, Tribological properties of PEO nanocomposite coatings on titanium formed in electrolyte containing ketoconazole, Tribol. Int. 102 (2016) 463–471.
[39] X. Nie, A. Leyland, H. Song, A. Yerokhin, S. Dowey, A. Matthews, Thickness effects on the mechanical properties of micro-arc discharge oxide coatings on aluminium alloys, Surf. Coat. Technol. 116 (1999) 1055–1060.
[40] A. Leyland, A. Matthews, On the significance of the H/E ratio in wear control: a nanocomposite coating approach to optimised tribological behaviour, Wear 246 (2000) 1–11.